ELSEVIER

Contents lists available at ScienceDirect

# Journal of Theoretical Biology

journal homepage: www.elsevier.com/locate/yjtbi





# Modeling the effects of drugs of abuse on within-host dynamics of two HIV species

Peter M. Uhl, Naveen K. Vaidya\*

Computational Science Research Center, San Diego State University, San Diego, CA, USA Department of Mathematics and Statistics, San Diego State University, San Diego, CA, USA Viral Information Institute, San Diego State University, San Diego, CA, USA

### ARTICLE INFO

#### Keywords: HIV Mutation Viral escape Morphine

### ABSTRACT

Injection drug use is one of the most significant risk factors associated with contracting human immunod-eficiency virus (HIV), and drug users infected with HIV suffer from a higher viral load and rapid disease progression. While replication of HIV may result in many mutant viruses that can escape recognition of the host's immune response, the presence of morphine (a drug of abuse) can decrease the viral mutation rate and cellular immune responses. This study develops a mathematical model to explore the effects of morphine-altered mutation and cellular immune response on the within-host dynamics of two HIV species, a wild-type and a mutant. Our model predicts that the morphine-altered mutation rate and cellular immune response allow the wild-type virus to outcompete the mutant virus, resulting in a higher set point viral load and lower CD4 count. We also compute the basic reproduction numbers and show that the dominant species is determined by morphine concentration, with the mutant dominating below and the wild-type dominating above a threshold. Furthermore, we identified three biologically relevant equilibria, infection-free, mutant-only, and coexistence, which are completely characterized by the fitness cost of mutation, mutant escape rate, and morphine concentration.

#### 1. Introduction

Human immunodeficiency virus (HIV) is a significant health concern worldwide, with 37.7 million infected people globally in 2021 (UNAIDS, 2021). In addition to sexual contact, HIV transmission is also commonly associated with recreational drug use through needle sharing between drug users (Alcabes and Friedland, 1995; Fauci, 2007). Drug use has also been shown to have several detrimental effects on people infected with HIV, such as a higher viral load, a more rapid progression to AIDS, a greater chance of HIV-related neurological complications, and an overall higher mortality rate (Kohli et al., 2005; Li et al., 2002; Kumar et al., 2004; Hauser et al., 2009). Therefore, it is essential to study how the conditioning of drugs of abuse affects the progression of HIV infections.

HIV replicates within target CD4+ T-cells. Individual virions bind to the target cell membrane, enter the target cell, replicate viral RNA, and then the infected cell releases the newly produced virus into the environment (Kitchen et al., 2005; Kileen et al., 1993; Chan and Kim, 1998). One of the defense mechanisms the host implements is a cellular immune response in the form of cytotoxic T-lymphocytes (CTLs), which are able to detect and kill infected cells by recognizing epitopes on the

surface of infected cells, thereby limiting viral replication (Greenough et al., 1997; Ganusov et al., 2013). The virus replication process is highly error-prone, resulting in many mutations (Klein et al., 1998). Many mutant viruses express epitopes different from wild-type viruses and escape detection by CTLs (Chan and Kim, 1998; Klein et al., 1998; Fryer et al., 2010). Pressure to escape CTLs, combined with the high turnover of virions and infected cells, plays a significant role in allowing HIV to establish infection (Ribeiro et al., 2010; Boutwell et al., 2010; McMichael and Rowland-Jones, 2001) and poses a major challenge in the control of the infection by immune responses, thereby causing obstacles in developing successful CTL-based vaccines (Deng et al., 2015; Konrad et al., 2011; Barouch et al., 2003).

Animal models with SIV (Simian Immunodeficiency Virus) in rhesus macaques have demonstrated several adverse effects that drugs of abuse can have on the prognosis of infection. In the experiment by Kumar et al. (2004), morphine-addicted animals were found to have decreased CD4+ T-cell count and increased set-point viral load compared to non-addicted animals. Many experimental studies have demonstrated the three major effects of drugs of abuse on the dynamics of HIV/SIV: (i) Drugs of abuse have been shown to increase expression of the

<sup>\*</sup> Correspondence to: 5500 Campanile Dr, San Diego, CA 92182, USA. E-mail address: nvaidya@sdsu.edu (N.K. Vaidya).

CCR5 co-receptor in target cells, making them more susceptible to infection (Li et al., 2002; Kumar et al., 2004; Miyagi et al., 2010); (ii) Opiates are known to diminish cellular immune responses (Rivera-Amill et al., 2014; Fuggetta et al., 2005); and (iii) the conditioning of the drugs of abuse is negatively correlated with SIV viral evolution and disease progression (Noel et al., 2006; Noel and Kumar, 2007; Rivera-Amill et al., 2014), indicating a lower mutation rate in the presence of drugs of abuse. While there is ample experimental evidence for these effects, their quantitative understanding is minimal. Therefore, the potential combined alteration in mutation, immune response, and cell susceptibility due to drugs of abuse need to be considered to quantify the effects of opiate use on HIV infections.

Mathematical models have been previously used to study infectious diseases, including HIV/SIV (Ganusov et al., 2013; Konrad et al., 2011; Perelson and Ribeiro, 2013; Chubb and Jacobsen, 2010; Conway and Perelson, 2015; Schwartz et al., 2016; Vaidya et al., 2016; Mutua et al., 2019; Ganusov and DeBoer, 2006; Ganusov et al., 2011). Models have also been developed to investigate viral escape (Ganusov and DeBoer, 2006; Ganusov et al., 2011, 2013), antibody responses (Mutua et al., 2019), viral evolution (Konrad et al., 2011), and cellular immune responses (Fryer et al., 2010; Althaus and DeBoer, 2008; Asquith et al., 2006; Fernandez et al., 2005; Schwartz et al., 2013). In this study, we present a mathematical model of HIV infection that incorporates morphine effects on the dynamics of viral replication, cellular immune responses, and mutation. We analyze the model to determine how morphine affects viral mutation and the long-term dynamics of mutant and wild-type virus species. We were able to fully characterize the dynamics using three steady state solutions of the model: an infectionfree steady state, a mutant-only steady state, and a coexistence steady state. Furthermore, we were able to show that the concentration of morphine present within the host is critical for the stability of the steady states of the virus-immune dynamical system.

#### 2. Method

# 2.1. Mathematical model

# 2.1.1. Virus-cell dynamics

We extend the standard HIV dynamics model (Perelson and Ribeiro, 2013; Schwartz et al., 2016) to include morphine effects on target cell susceptibility, viral mutation, and cellular immune response, which have been established in various experimental studies (Li et al., 2002; Kumar et al., 2004; Noel et al., 2006; Noel and Kumar, 2007; Rivera-Amill et al., 2014; Fuggetta et al., 2005; Miyagi et al., 2010). Following Vaidya et al. (2016) and Mutua et al. (2019), we include two populations of CD4+ target cells based on levels of CCR5 co-receptor expression: a population with lower susceptibility to infection,  $T_l$ , and a population with higher susceptibility to infection,  $T_h$  (Li et al., 2002; Kumar et al., 2004; Miyagi et al., 2010). The viral mutation is modeled by including two viral species, a wild-type virus,  $V_w$ , and a mutant virus,  $V_m$  (Klein et al., 1998; McMichael and Rowland-Jones, 2001). We assume free virus particles infect target cells, resulting in corresponding infected cell populations,  $I_w$  and  $I_m$ . Cellular immune responses are represented by a population of CTLs, denoted by C, which directly kills infected cells (Konrad et al., 2011; DeBoer and Perelson, 1998).

Target cells are recruited at a constant rate  $\lambda$  and are assumed to belong to the  $T_l$  population. Target cells switch from  $T_l$  to  $T_h$  at rate r and from  $T_h$  to  $T_l$  at rate q (Vaidya et al., 2016). Both populations of target cells die at per capita rate  $\delta_T$  (Perelson and Ribeiro, 2013; Schwartz et al., 2016). Target cells in the  $T_l$  population are infected by the wild-type virus at rate  $\beta_l$  and by the mutant virus at a rate  $(1-F)\beta_l$ , where F denotes the fitness cost of mutation, with  $0 \le F \le 1$ . Note that we assume the mutant virus to have a lower infection rate than the wild-type virus (Ganusov et al., 2011). Similarly,  $T_h$  cells are infected at rates  $\beta_h$  and  $(1-F)\beta_h$  by the wild-type and mutant viruses, respectively. Due to mutation, a fraction  $\epsilon$  of target cells infected by wild-type virus

become mutant-infected cells, and the remaining  $(1 - \epsilon)$  stay wild-type infected cells (Konrad et al., 2011).

Both virus species are produced by their corresponding infected cell population at rate p per cell and are cleared at rate  $\delta_V$  (Konrad et al., 2011). We consider only forward mutation, i.e., target cells infected by the mutant virus do not revert to the wild-type infected population because the back mutation in the presence of morphine is not understood well. Wild-type infected cells,  $I_w$ , are killed by CTLs at rate b. Due to responses by epitope-specific CTLs, there is a reduced recognition of mutant-infected cells by the host's immune responses (Konrad et al., 2011; Barouch et al., 2003). We interpret this reduced rate as the escape rate. CTLs kill  $I_m$  cells at rate  $\frac{b}{1+B}$ , in which the base CTL killing rate b is reduced by the mutant escape ratio 1 + B. The mutant escape rate, B > 0, represents a reduction in the ability of the host's cellular immune response to kill cells infected by the mutant virus compared to cells infected by the wild-type virus. Both classes of infected cells die at per capita rate  $\delta_I$ . CTLs are produced at rate  $\alpha$  per infected cell (Konrad et al., 2011; DeBoer and Perelson, 1998), die at rate  $\delta_C$ , and recruited at a constant rate  $\omega$  (Conway and Perelson, 2015), which also includes background production other than those proportional to infected cells.

#### 2.1.2. Effects of morphine

Based on experimental results, we include the effects of morphine through three mechanisms: the higher transfer of  $T_l$  cells into  $T_h$  cells due to increased co-receptor expression (Kumar et al., 2004; Miyagi et al., 2010), the decrease in viral mutation (Noel et al., 2006; Noel and Kumar, 2007), and the decrease in CTL production (Rivera-Amill et al., 2014). We, therefore, make the transition parameters r and q morphine-dependent, i.e., r = r(M) and q = q(M), where M is the concentration of morphine. Since it is expected that r(M) is an increasing function of morphine and q(M) is a decreasing function of morphine, we model r(M) and q(M) using an  $E_{max}$  model as done previously (Vaidya and Peter, 2021),

$$r(M) = r_c + (r_m - r_c)\eta_r(M),$$
  

$$q(M) = q_m + (q_c - q_m)\eta_q(M),$$
(1)

where

$$\eta_r(M) = \frac{M^n}{M_h^n + M^n},$$
 
$$\eta_q(M) = 1 - \eta_r(M).$$
 (2)

Here,  $r_c$  and  $r_m$  are the minimum and maximum values of r(M),  $q_c$  and  $q_m$  are the minimum and maximum values of q(M), n is Hill's coefficient for the  $E_{max}$  model, and  $M_h$  is the morphine concentration that gives r(M) and q(M) the value half-way between their respective minimums and maximums. Since morphine causes a decrease in viral mutation (Noel et al., 2006; Noel and Kumar, 2007), we model the mutation rate as  $\frac{\epsilon}{\mu+\eta M}$ , where  $\mu$  and  $\eta$  are parameters related to the effect of morphine on mutation. To model the decrease in CTL production due to morphine, we take the CTL recruitment rate as  $\omega e^{-\psi M}$  and the CTL production rate in response to infection as  $\frac{\alpha}{\gamma+\xi M}$ , where  $\psi$ ,  $\gamma$ , and  $\xi$  are parameters related to the decrease in CTL production due to morphine. The full model is given by the following seven-dimensional system of ODEs:

$$\begin{split} \frac{dT_l}{dt} &= \lambda + \left(q_m + (q_c - q_m) \left(1 - \frac{M^n}{M_h^n + M^n}\right)\right) T_h \\ &- \left(r_c + (r_m - r_c) \frac{M^n}{M_h^n + M^n}\right) T_l \\ &- \beta_l V_w T_l - (1 - F) \beta_l V_m T_l - \delta_T T_l, \\ \frac{dT_h}{dt} &= \left(r_c + (r_m - r_c) \frac{M^n}{M_h^n + M^n}\right) T_l \\ &- \left(q_m + (q_c - q_m) \left(1 - \frac{M^n}{M_h^n + M^n}\right)\right) T_h \\ &- \beta_h V_w T_h - (1 - F) \beta_h V_m T_h - \delta_T T_h, \end{split}$$

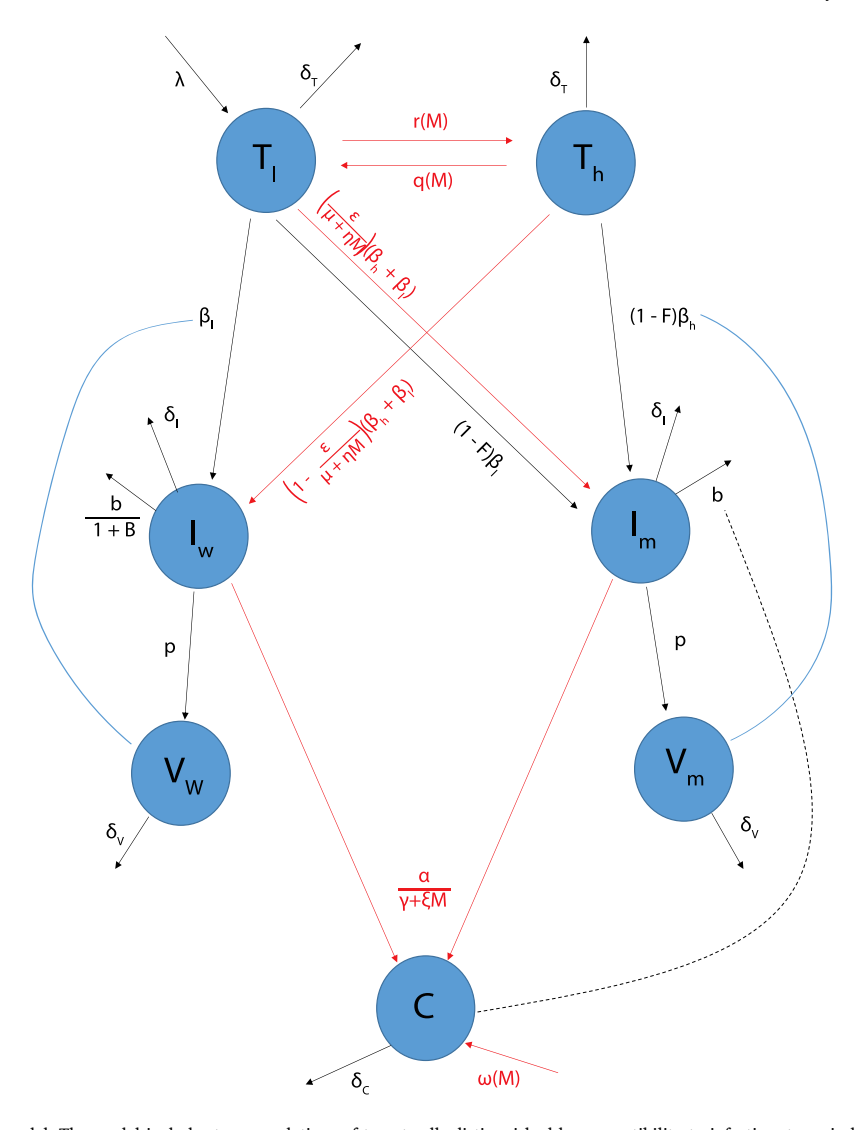


Fig. 1. Schematic diagram of the model. The model includes two populations of target cells distinguished by susceptibility to infection, two viral strains and corresponding infected populations, and a cellular immune response in the form of CTLs. Viral species are distinguished by their infectivity rates and ability to escape from immune responses. Mechanisms that are affected by morphine, shown by red arrows, are the rate of viral mutation, target cell susceptibility, and production rate of CTLs.

$$\begin{split} \frac{dV_w}{dt} &= pI_w - \delta_V V_w, \\ \frac{dV_m}{dt} &= pI_m - \delta_V V_m, \\ \frac{dI_w}{dt} &= pI_m - \delta_V V_m, \\ \frac{dI_w}{dt} &= \left(1 - \frac{\epsilon}{\mu + \eta M}\right) (\beta_l V_w T_l + \beta_h V_w T_h) - bI_w C - \delta_I I_w, \\ \frac{dI_m}{dt} &= \frac{\epsilon}{\mu + \eta M} (\beta_l V_w T_l + \beta_h V_w T_h) + (1 - F)(\beta_l V_m T_l + \beta_h V_m T_h) \\ &- \frac{b}{1 + B} I_m C - \delta_I I_m, \\ \frac{dC}{dt} &= \omega e^{-\psi M} + \frac{\alpha}{\gamma + \xi M} (I_w + I_m) C - \delta_C C. \end{split}$$

A schematic diagram of the model is shown in Fig. 1.

# 2.2. Parameter estimation

We obtained some parameters from the literature and estimated some parameter values based on previously published studies. Following Vaidya et al. (2016), we assume  $10^6$  target cells per ml of blood, with 40 980 cells/ml belonging to the  $T_h$  population and the remaining 959 020 cells/ml to the  $T_l$  population. We assume that the infection begins with free virus only, and there are no infected cells, so we take  $I_w(0)$ ,  $I_m(0) = 0$ . Also, as described in Vaidya et al. (2016), the

SIV infection was established with  $3 \times 10^5$  RNA copies of the virus. Assuming a macaque contains approximately 1.5 liters of extracellular water, we can estimate  $V_0 = \frac{3\times 10^5}{1.5L} \approx 200$  viral RNA copies/ml (Vaidya et al., 2016), which we assume to belong entirely to the  $V_{\iota\nu}$  population. Estimates for  $\lambda$ ,  $\beta_l$ ,  $\beta_h$ ,  $r_c$ ,  $r_m$ ,  $q_m$ ,  $q_c$ , and  $\delta_I$  were taken from Vaidya et al. (2016), where these values were obtained by fitting the model to experimental data. In particular, they estimated  $\beta_h$  to be approximately two orders of magnitude higher than  $\beta_l$ . The viral production rate, p, is estimated from the SIV in vivo burst size in rhesus macaques and the average life span of an infected cell, giving p=2500 per cell/day (Vaidya et al., 2016).

Based on modeling work by Stafford et al. (2000), we take  $\delta_T=1/100=0.01$  per day, corresponding to a target cell life span of 100 days. Ramratnam et al. (1999) give an estimated range of HIV viral clearance between 9.1 and 36 virions per day, so we use their average of 23 virions per day as our base value for  $\delta_V$ . Mansky and Temin (1995) determined the *in vivo* mutation rate of HIV-1 to be  $3.4\times10^{-5}$  mutations per base pair per generation, so we take the mutation rate  $\epsilon=3\times10^{-5}$ . Following DeBoer and Perelson (DeBoer and Perelson, 1998), we take  $\delta_C=0.2$  per day as an estimate for the turnover of CTLs and  $\alpha/\gamma=6.7\times10^{-5}$  for the infected cell-dependent CTL production rate. Similar to other modeling works, we also include a constant production of CTLs  $\omega=15$  to include potential background

Table 1

Parameter	Value (Range for LHS)	Description	Reference
λ	3690 (1500, 10000) ml/day	Production rate of $T_l$ cells	Vaidya et al. (2016)
r(M)	$r_c + (r_m - r_c)\eta_r(M) \ (0.005, 2.7)$	Transition rate from $T_l$ to $T_h$	Vaidya et al. (2016)
q(M)	$q_c + (q_m - q_c)\eta_q(M) \ (10^{-8}, 2.8)$	Transition rate from $T_h$ to $T_l$	Vaidya et al. (2016)
$r_c$	0.16 day <sup>-1</sup>	Minimum value of $r$	Vaidya et al. (2016)
$r_m$	$0.52   \mathrm{day^{-1}}$	Maximum value of $r$	Vaidya et al. (2016)
$q_c$	$1.23 \times 10^{-6} \text{ day}^{-1}$	Minimum value of $q$	Vaidya et al. (2016)
$q_m$	$0.25  day^{-1}$	Maximum value of $q$	Vaidya et al. (2016)
$M_h$	100 μg/l	Half morphine value for $r(M)$ , $q(M)$	Olkkola et al. (1988)
n	8	Hill's coefficient of morphine response	Vaidya et al. (2016)
$\beta_l$	$10^{-9} (10^{-11}, 10^{-5}) \text{ ml/day}$	Wild- type infection rate of $T_l$ cells	Vaidya et al. (2016)
$\beta_h$	$10^{-7} (10^{-9}, 10^{-3}) \text{ ml/day}$	Wild -type infection rate of $T_h$ cells	Vaidya et al. (2016)
F	0.1 (0-1)	Fitness cost of mutation	Assumed
p	2500 (500, 5500) day <sup>-1</sup>	Production rate of virus	Vaidya et al. (2016)
b	0.25 (0.005, 1.8) ml/day	CTL killing rate of wild-type	Ganusov et al. (2011)
В	30 (0.1, 100)	Mutant escape ratio	Assumed
α	$6.7 \times 10^{-5} \text{ ml/day}$	CTL response to infection	DeBoer and Perelson (1998
γ	1	Morphine effect on $\alpha$	Assumed
ξ	1 l/μg	Morphine effect on $\alpha$	Assumed
ω	15 (0.001, 40) ml/day	Base CTL production rate	Assumed
Ψ	0.1 (0.001, 1.5) ml/day	CTL production decay rate	Assumed
$\epsilon$	$3 \times 10^{-5} \ (3 \times 10^{-7}, 3 \times 10^{-3})$	Mutation rate	Mansky and Temin (1995)
μ	1 (0.01, 50)	Morphine effect on $\epsilon$	Assumed
η	1 (0.01, 50) 1/μg	Morphine effect on $\epsilon$	Assumed
$\delta_T$	0.01 (0.001, 1.2) day <sup>-1</sup>	Target cell death rate	Stafford et al. (2000)
$\delta_V$	23 (1,50) day <sup>-1</sup>	Virus clearance rate	Ramratnam et al. (1999)
$\delta_I$	0.7 (0.01, 10) day <sup>-1</sup>	Infected cell death rate	Vaidya et al. (2016)
$\delta_C$	0.2 (0.001, 1.6) day <sup>-1</sup>	CTL death rate	DeBoer and Perelson (1998
M	$0 - 200  \mu g/1$	Concentration of morphine	Olkkola et al. (1988)

production other than those proportional to infected cells (Conway and Perelson, 2015; Adams et al., 2005; Tarfulea, 2017).

Previous work by Ganusov et al. (2011) investigated the rate of escape by mutant viruses from CTL responses. They measured the rate of escape by a single mutant variant as the average difference between the rate of mutant killing by CTLs and the production rate of the mutant. They consider the range of killing of infected cells (wild-type and mutant) by CTLs to be 0.01–0.5 per day, so we take b=0.25 per day as our base value. In their study, the upper-value b=0.5 corresponds to a wild-type virus, and the lower-value b=0.01 to an escape mutant. Noting that  $\frac{0.5}{0.01}=50$ , we will vary the escape ratio, B, from 0 to 50 with B=30 as our base value (Ganusov et al., 2011).

In an experiment performed on children aged between two and six years, Olkkola et al. (1988) observed initial morphine concentrations between 28 and 325  $\mu$ g/l of blood plasma. To include this range, we will consider values of M to be between 0 and 200  $\mu$ g/l (Olkkola et al., 1988). Accordingly, we take  $M_h=100$ , corresponding to the half-saturation value of r(M) and q(M). The estimated parameters and their descriptions are summarized in Table 1.

#### 3. Results

#### 3.1. Basic reproduction number

The basic reproduction number, denoted by  $R_0$ , is defined as the average number of secondary infected cells resulting from a single initial infected cell when target cells are not limited (Castillo-Chavez et al., 2002).  $R_0$  is an important quantity in the study of viral dynamics that provides a threshold condition for infection to persist ( $R_0 > 1$ ) and to die out ( $R_0 < 1$ ).

We use the next-generation matrix method (Diekmann et al., 2009) to obtain an expression for the basic reproduction number of our model. The next-generation matrix is obtained from the infected subsystem of the model, i.e., the equations of the system corresponding to viruses

and infected cells (Diekmann et al., 2009). For our model, the infected subsystem is given by

$$\begin{split} \frac{dV_w}{dt} &= pI_w - \delta_V V_w, \\ \frac{dV_m}{dt} &= pI_m - \delta_V V_m, \\ \frac{dI_w}{dt} &= (1 - \hat{\epsilon}(M))(\beta_l V_w T_l + \beta_h V_w T_h) - bI_w C - \delta_I I_w, \\ \frac{dI_m}{dt} &= \hat{\epsilon}(M)(\beta_l V_w T_l + \beta_h V_w T_h) + (\hat{\beta}_l V_m T_l + \hat{\beta}_h V_m T_h) \\ &- \frac{b}{1+B} I_m C - \delta_I I_m, \end{split} \tag{4}$$

where  $\hat{\epsilon}(M) = \frac{\epsilon}{\mu + \eta M}$ ,  $\hat{\beta}_l = (1 - F)\beta_l$ , and  $\hat{\beta}_h = (1 - F)\beta_h$ . The infection-free equilibrium (IFE) is the steady-state solution of the model, in which all infected cell and virus populations are zero. For our model, we compute the IFE as  $(T_i^*, T_k^*, 0, 0, 0, 0, C^*)$ , where

$$\begin{split} T_l^* &= \frac{\lambda(q(M) + \delta_T)}{\delta_T(q(M) + r(M) + \delta_T)}, \\ T_h^* &= \frac{\lambda r(M)}{\delta_T(q(M) + r(M) + \delta_T)}, \\ C^* &= \frac{\dot{\phi}(M)}{\delta_C}, \end{split} \tag{5}$$

and  $\hat{\omega}(M) = \omega e^{-\psi M}$ . Now, we linearize the infected subsystem about the IFE and decompose it into  $\mathcal{F} - \mathcal{V}$ , where  $\mathcal{F}$  is the part of the system that describes newly infected components, and  $\mathcal{V}$  is the part that describes transitions of cells and viruses in and out of compartments.  $\mathcal{F}$  and  $\mathcal{V}$  for our model are given by

$$\mathcal{F} = \begin{bmatrix} 0 & 0 & 0 & 0 & 0 \\ 0 & 0 & 0 & 0 & 0 \\ (1 - \hat{\epsilon}(M))(\beta_l T_l^* + \beta_h T_h^*) & 0 & 0 & 0 \\ \hat{\epsilon}(M)(\beta_l T_l^* + \beta_h T_h^*) & (\hat{\beta}_l T_l^* + \hat{\beta}_h T_h^*) & 0 & 0 \end{bmatrix}$$
(6)

and

$$\mathcal{V} = \begin{bmatrix}
\delta_V & 0 & -p & 0 \\
0 & \delta_V & 0 & -p \\
0 & 0 & \delta_I + bC^* & 0 \\
0 & 0 & 0 & \delta_I + \frac{b}{1+B}C^*
\end{bmatrix}.$$
(7)

The next-generation matrix is  $\mathcal{FV}^{-1}$  (Diekmann et al., 2009). The basic reproduction number of our model is then obtained as the spectral radius of  $\mathcal{FV}^{-1}$ , i.e.,  $R_0 = \sigma(\mathcal{FV}^{-1}) = \max\{R_0^w, R_0^m\}$ , where

$$\begin{split} R_0^w &= \frac{(1-\hat{\epsilon}(M))(\beta_h T_h^* + \beta_l T_l^*)p}{\delta_V(bC^* + \delta_I)} \quad \text{and} \\ R_0^m &= \frac{(1-F)(\beta_h T_h^* + \beta_l T_l^*)(1+B)p}{\delta_V(\delta_I B + bC^* + \delta_I)} \end{split}$$

represent the basic reproduction number corresponding to the wild-type and mutant virus, respectively. Note that since  $\hat{e}(M), T_l^*, T_h^*$ , and  $C^*$  are morphine dependent,  $R_0^w$  and  $R_0^m$  are also morphine dependent. In addition, if  $R_0^w < 1$  and  $R_0^m < 1$  the infection will die out while if either  $R_0^w > 1$  or  $R_0^m > 1$  the infection will be established (Castillo-Chavez et al., 2002). Using the parameter values in Table 1, we compute  $R_0^w = 0.08$ ,  $R_0^m = 1.07$ , and  $R_0 = max\{R_0^w, R_0^m\} = 1.07 > 1$ , indicating that the infection persists for this basic parameter set.

To study the effect of each parameter on  $R_0$ , we first determine the local sensitivity of  $R_0^w$  and  $R_0^m$  to changes in individual parameters. For a parameter  $\rho$  of the model, the forward sensitivity index is given by

$$S_{\rho} = \frac{\rho}{R_0} \frac{\partial R_0}{\partial \rho}.$$
 (9)

Then  $S_a$  determines the relative instantaneous change in  $R_0$  caused by a change in  $\rho$  (Marino et al., 2008; Perera et al., 2006; Rodrigues et al., **2013).** The higher the values of  $S_{\rho}$ , the more sensitive  $R_0$  is to  $\rho$ . Also, positive (negative) values of  $S_{\rho}$  indicate that  $R_0$  increases (decreases) as  $\rho$  increases. Sensitivity indices for  $R_0^w$  and  $R_0^m$  are shown in Fig. 2 (left). We found that  $R_0^w$  and  $R_0^m$  are positively correlated to  $\lambda, r, p$ , and  $\delta_C$ , indicating that an increase in these parameters is favorable for an infection to occur. This is expected since increasing  $\lambda$ , r, and  $\delta_C$  will result in more (susceptible) target cells available for infection while increasing p results in more virions that can infect target cells. On the other hand,  $R_0^w$  and  $R_0^m$  are negatively correlated to  $q,\ b,\ \delta_T,\delta_V,$  and  $\omega$ . Increased  $\delta_T$  and  $\delta_V$  cause increased death of target cells and viral clearance, respectively, both unfavorable for the virus, while a larger  $\omega$  means more CTLs are responding to the infection. Larger values of parameter q increase target cells in the lower susceptible population, and increased CTL killing rate *b* indicates a stronger immune response. Both of these mechanisms are also unfavorable to the virus. In addition,  $R_0^m$  is positively related to B and negatively related to F since a mutant virus benefits from a higher rate of immune escape and lower fitness of mutation. We found that  $R_0^w$  and  $R_0^m$  are less sensitive to changes in  $\beta_l$ ,  $\beta_h$ ,  $\epsilon$ ,  $\mu$ ,  $\eta$  or  $\psi$  on these base-case parameters.

To further quantify the global sensitivity of  $R_0^w$  and  $R_0^m$  to the parameters, we used Latin hypercube sampling (LHS) to obtain 10,000 samples of parameter sets. We used these parameters to calculate corresponding  $R_0^w$  and  $R_0^m$  values. In LHS, individual parameter values were sampled uniformly from the interval  $[\rho_{min}, \rho_{max}]$  for each parameter  $\rho$ , where  $\rho_{min}$  and  $\rho_{max}$  were selected to give a realistic range of values (Table 1). The PRCCs of rank-transformed data were then calculated as the Pearson correlation coefficient between the vectors of residuals from the two regression models (the regression between the reproductive number and the remaining parameters and the regression between the selected parameter and the remaining parameters) (Marino et al., 2008).

The obtained partial rank correlation coefficients are shown in Fig. 2 (right). The LHS-based sensitivities are consistent with the forward sensitivity indices, but the magnitude of sensitivity is relatively lower in general. Here also,  $\lambda, r, p$ , and  $\delta_C$ , i.e., those related to increased

amounts of virus and susceptible target cells, are mostly associated with more infectious viruses. Similarly, higher values of the CTL killing rate b, death rates  $\delta_T, \delta_V, \delta_I$ , and CTL production rate  $\omega$  lead to fewer viruses. Note that  $R_0^\omega$  is unaffected by changes in F and B since these parameters only relate to the viability of the mutant virus. The mutant benefits from a low fitness cost and high rate of immune escape, which is reflected in  $R_0^m$  being positively associated with B and negatively associated with F.

#### 3.2. Virus species switch

The viral species with a larger reproduction number can be considered to be the dominant species. For the base case with M=0 we obtained  $R_0^w=0.08$  and  $R_0^m=1.07$ , indicating that the mutant is the dominant viral population. An increase in M increases both  $R_0^w$  and  $R_0^m$ , and so  $R_0$ . For example, M=200 causes  $R_0^w$ ,  $R_0^m$ , and  $R_0$  to become 5.6, 5.05, and 5.6, respectively. We found that increasing the amount of morphine past a threshold value,  $M_{thresh}$ , results in a viral species switch. The wild-type becomes the dominant viral population when the morphine concentration exceeds  $M_{thresh}$  (Fig. 3).

The value of  $M_{thresh}$  can be determined by solving  $R_0^w(M) = R_0^m(M)$  for M. For  $M < M_{thresh}$ , the mutant dominates, and for  $M > M_{thresh}$ , the wild-type dominates. Due to the nonlinearity in  $R_0^w$  and  $R_0^m$ , we did not find a closed form for  $M_{thresh}$  and obtained it numerically. For our base parameter values,  $M_{thresh} \approx 54$ , the wild-type is the dominant population for M > 54, and the mutant dominates for M < 54.

We now evaluate the effect of F (fitness cost) and B (immune escape) on  $M_{thresh}$ . As predicted by our model (Fig. 3), in general,  $M_{thresh}$  decreases as F increases and/or B decreases. For a substantially higher fitness cost (for example, F > 0.93 in our computations), the mutant population is not fit enough to out-compete the wild-type, and the wild-type always dominates for any values of M. On the other hand, for a low enough B (B < 0.12 in our computations), we did not find any value of  $M_{thresh}$  because CTLs are highly effective against the mutant virus, and the mutant virus cannot out-compete the wild-type virus.

# 3.3. Stability of steady-states

### 3.3.1. Infection-free equilibrium

The IFE is shown in Section 3.1. As discussed earlier, the local stability of the IFE is determined by the basic reproduction number. It is easy to prove that the IFE is locally asymptotically stable if  $R_0 < 1$  and unstable if  $R_0 > 1$  (Castillo-Chavez et al., 2002).

# 3.3.2. Wild-type only equilibrium

A wild-type only equilibrium is a solution,  $(T_l^*, T_h^*, V_w^*, 0, I_w^*, 0, C^*)$ , of the following system of equations

$$0 = \lambda + q(M)T_{h}^{*} - r(M)T_{l}^{*} - \beta_{l}V_{w}^{*}T_{l} - \delta_{T}T_{l}^{*},$$

$$0 = r(M)T_{l}^{*} - q(M)T_{h}^{*} - \beta_{h}V_{w}^{*}T_{h}^{*} - \delta_{T}T_{h}^{*},$$

$$0 = pI_{w}^{*} - \delta_{V}V_{w}^{*},$$

$$0 = (1 - \hat{\epsilon}(M))(\beta_{l}V_{w}^{*}T_{l} + \beta_{h}V_{w}^{*}T_{h}^{*}) - bI_{w}^{*}C^{*} - \delta_{I}I_{w}^{*},$$

$$0 = \hat{\epsilon}(M)(\beta_{l}V_{w}^{*}T_{l}^{*} + \beta_{h}V_{w}^{*}T_{h}^{*}),$$

$$0 = \hat{\omega}(M) + \hat{\alpha}(M)I_{w}^{*}C - \delta_{C}C^{*}.$$

$$(10)$$

Solving the second equation for  $T_h^*$  gives:

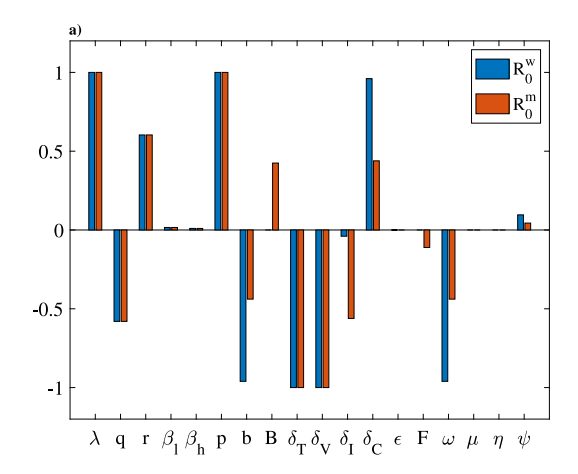
$$T_h^* = \frac{r(M)}{q(M) + \beta_h V_w^* + \delta_T} T_l^*, \tag{11}$$

and, since  $\hat{\epsilon}(M) \neq 0$ , the fifth equation is equivalent to

$$0 = \beta_l V_w^* T_l^* + \beta_h V_w^* T_h^*. \tag{12}$$

This implies  $V_w^* = 0$ , which corresponds to the IFE, or

$$0 = T_l^* \left( \beta_l + \beta_h \left( \frac{r(M)}{q(M) + \beta_h V_w^* + \delta_T} \right) \right). \tag{13}$$



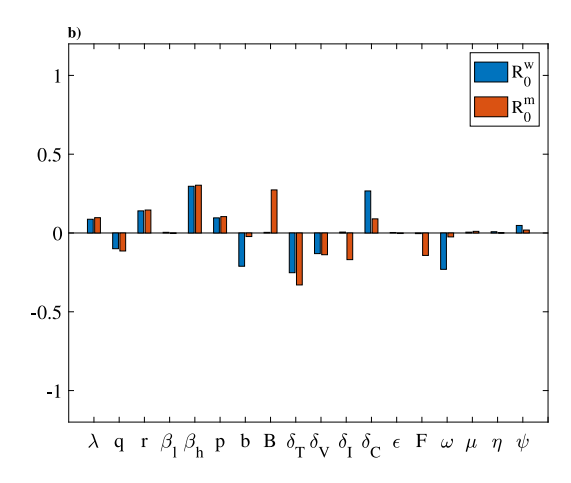
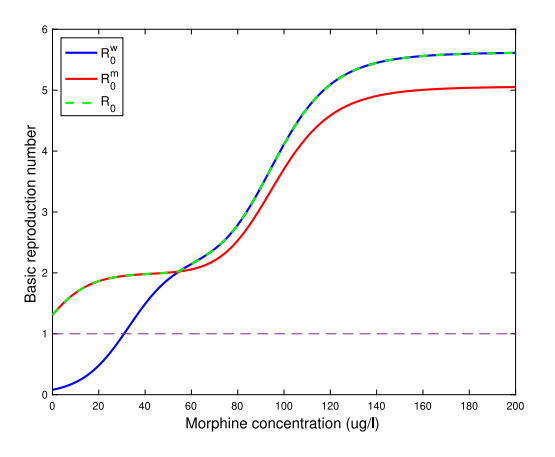


Fig. 2. Local sensitivity indices (left) and partial rank correlation coefficients from 10,000 LHS for  $R_0^w$  and  $R_0^m$ . A positive value is favorable to the virus infection while a negative value is unfavorable to the viral infection. The higher the magnitude of the sensitivity value, the more sensitive  $R_0$  is to the parameter.



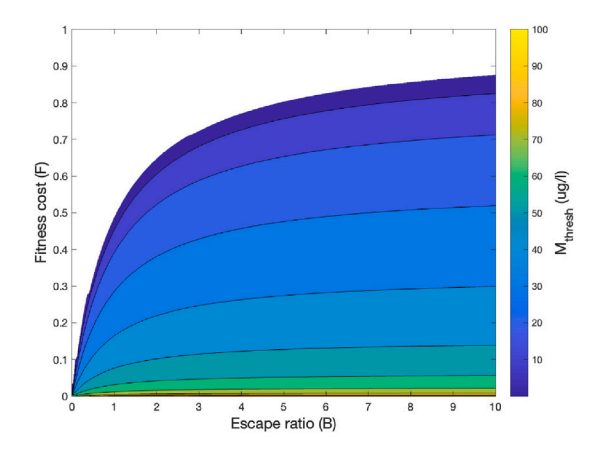


Fig. 3. (Left)  $R_0^w$  and  $R_0^m$  as functions of M. With parameter values as in Table 1,  $M_{thresh} \approx 54 \,\mu\text{g/ml}$ . The mutant is the dominant population for  $M < 54 \,\mu\text{g/ml}$  and the wild-type is dominant for  $M > 54 \,\mu\text{g/ml}$ . (Right)  $M_{thresh}$  in F - B parameter space. An increase in fitness cost (F) or a decrease in escape ratio B causes an increase in  $M_{thresh}$  value. The upper-left region represents (F, B) values that cause the wild-type to always dominate.

Then either  $T_l^*=0$  or  $\beta_l+\beta_h(\frac{r(M)}{q+\beta_hV_w^*+\delta_T})=0$ . Substituting  $T_l^*=0$  into the first equation gives the negative solution  $T_h^*=-\frac{\lambda}{q(M)}$ . Also, letting  $\beta_l+\beta_h(\frac{r(M)}{q(M)+\beta_hV_w^*+\delta_T})=0$ , we get

$$V_w^* = -\frac{1}{\beta_h} \left( \frac{\beta_h r(M)}{\beta_l} + q(M) + \delta_T \right), \tag{14}$$

which is also a negative solution. Therefore, the system does not provide a wild-type only equilibrium. This is expected because the wild-type virus promotes a fraction of infections transitioned to the mutant population due to de novo mutation.

## 3.3.3. Mutant-only equilibrium

The mutant only equilibrium (MOE) is the steady-state solution of the model, in which only the mutant population exists. The MOE of our model takes the form  $(\hat{T}_l, \hat{T}_h, 0, \hat{V}_m, 0, \hat{I}_m, \hat{C})$ , where

$$\begin{split} \hat{T_h} &= \frac{r(M)\lambda}{(q(M) + \hat{\beta}_h \hat{V}_m + \delta_T)(r(M) + \hat{\beta}_l \hat{V}_m + \delta_T) - r(M)q(M)}, \\ \hat{T_l} &= \frac{\lambda(q(M) + \hat{\beta}_h \hat{V}_m + \delta_T)}{(q(M) + \hat{\beta}_h \hat{V}_m + \delta_T)(r(M) + \hat{\beta}_l \hat{V}_m \delta_T) - r(M)q(M)}, \\ \hat{I_m} &= \frac{\delta_V \hat{V}_m}{p}, \\ \hat{C} &= \frac{\hat{\omega}(M)}{\delta_C - \hat{\alpha}} \frac{\delta_V \hat{V}_m}{p}, \end{split}$$
(15)

and 
$$\hat{V}_m$$
 is the solution of 
$$g(\hat{V}_m) = 0, \tag{16} \label{eq:16}$$
 with

$$\begin{split} g(\hat{V}_m) &= \frac{\hat{\beta}_l \hat{V}_m \lambda \left(\hat{V}_m \hat{\beta}_h + q(M) + \delta_T\right) + \hat{\beta}_h r(M) \hat{V}_m \lambda}{\left(\hat{V}_m \hat{\beta}_h + q(M) + \delta_T\right) \left(\hat{V}_m \hat{\beta}_l + r(M) + \delta_T\right) - r(M) q(M)} \\ &- \frac{b \delta_V \hat{V}_m \hat{\omega}}{(1+B) \, p \left(\delta_C - \frac{\hat{\alpha} \delta_V V_m^*}{p}\right)} - \frac{\delta_I \delta_V \hat{V}_m}{p}. \end{split}$$

Clearly,  $\hat{V}_m = 0$  is a solution that corresponds to the IFE. We now obtain solutions with  $\hat{V}_m > 0$ . We can obtain a value for  $\hat{V}_m$  by solving (16) numerically, and substituting into the expressions for  $\hat{T}_h, \hat{T}_l, \hat{I}_m$ , and  $\hat{C}$ . Geometrically,  $\hat{V}_m$  can be represented by the intersection of the curve  $g(\hat{V}_m)$  and the axis g=0. As shown in Fig. 4a, the steadystate value of  $\hat{V}_m$  at the MOE is the x-intercept of the curve  $g(\hat{V}_m)$ . We observe that the higher morphine concentrations intersect the xaxis further to the right. These  $\hat{V}_m$  values at MOE can be substituted into the expressions for the other variables at MOE. A graph of  $\hat{V}_m$ as a function of M (Fig. 4b) shows that increasing M causes a larger non-zero equilibrium value of  $\hat{V}_m$ , indicating a higher set point viral load for larger morphine concentrations, consistent with experimental results (Kumar et al., 2004). Moreover, increasing M reduces values of  $T_l, T_h$ , and C, and increases the value of  $I_m$  at the MOE (Fig. 4cf). Combining all these results, we conclude that morphine causes infection of more target cells and less killing of infected cells by CTLs at the MOE.

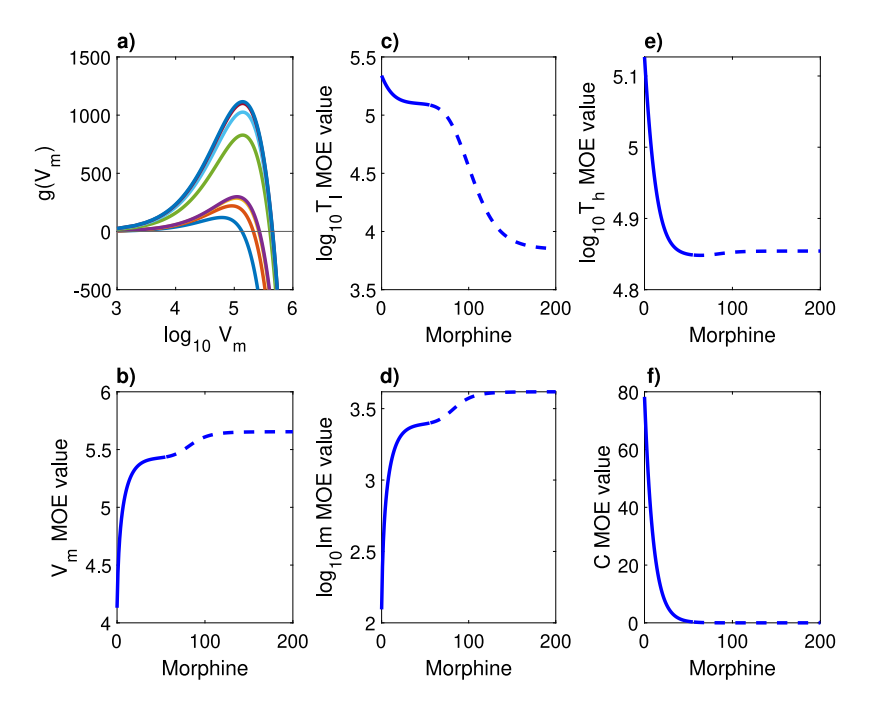


Fig. 4. (a) Graphs of  $g(V_m)$  (Eq. (16)) for different morphine levels. Each color represents a different value of M, and the x-intercept of each curve represents the steady-state viral load at the MOE. (b - f)  $V_m$ ,  $T_l$ ,  $T_n$ ,  $I_m$ , and C steady-state values at MOE. Morphine is varied along the x-axis, and the y-axis represents the steady-state value at the MOE. The solid portion of each curve represents locally-stable equilibria, and the dashed portions represent unstable equilibria.

To determine the local stability of the MOE, we calculate the eigenvalues of the Jacobian matrix, J, of the model evaluated at the MOE, given by

$$J = \begin{bmatrix} J_{11} & J_{12} & J_{13} & J_{14} & 0 & 0 & 0 \\ J_{21} & J_{22} & J_{23} & J_{24} & 0 & 0 & 0 \\ 0 & 0 & J_{33} & 0 & J_{35} & 0 & 0 \\ 0 & 0 & 0 & J_{44} & 0 & J_{46} & 0 \\ J_{51} & J_{52} & J_{53} & 0 & J_{55} & 0 & J_{57} \\ J_{61} & J_{62} & J_{63} & J_{64} & 0 & J_{66} & J_{67} \\ 0 & 0 & 0 & 0 & J_{57} & J_{57} \end{bmatrix},$$

$$(17)$$

where

$$\begin{array}{lllll} J_{11} & = & -r(M) - \beta_l V_w - \hat{\beta}_l V_m - \delta_T, & J_{52} & = & (1 - \hat{\epsilon}(M)) \beta_h V_w, \\ J_{12} & = & q(M), & J_{53} & = & (1 - \hat{\epsilon}(M)) (\beta_l T_l + \beta_h T_h), \\ J_{13} & = & -\beta_l T_l, & J_{55} & = & -bC - \delta_I, \\ J_{14} & = & -\hat{\beta}_l T_l, & J_{57} & = & -bI_w, \\ J_{21} & = & r(M), & J_{61} & = & \hat{\epsilon}(M) (\beta_l V_w + \hat{\beta}_l V_m), \\ J_{22} & = & -q(M) - \beta_h V_w - \hat{\beta}_h V_m - \delta_T, & J_{62} & = & \hat{\epsilon}(M) (\beta_l V_w + \hat{\beta}_l V_m), \\ J_{23} & = & -\beta_h T_h, & J_{63} & = & \hat{\epsilon}(M) (\beta_l T_l + \beta_h T_h), \\ J_{24} & = & -\hat{\beta}_h T_h, & J_{64} & = & \hat{\beta}_l T_l + \hat{\beta}_h T_h, \\ J_{33} & = & -\delta_V, & J_{66} & = & -\frac{b}{1+B}C - \delta_I, \\ J_{35} & = & p, & J_{67} & = & -\frac{b}{1+B}I_m, \\ J_{44} & = & -\delta_V, & J_{75} & = & \hat{\alpha}(M)C, \\ J_{46} & = & p, & J_{76} & = & \hat{\alpha}(M)C, \\ J_{51} & = & (1 - \hat{\epsilon})\beta_l V_w, & J_{77} & = & \hat{\alpha}(M)(I_w + I_m) - \delta_C. \end{array}$$

The MOE is locally asymptotically stable if the real part of each eigenvalue of J is negative and unstable otherwise (Perko, 1991; Jordan and Smith, 1999). We determined the stability of the MOE by computing the eigenvalues of J(MOE) for  $M \in [0,200]$ . We observed that each eigenvalue of J(MOE) had a negative real part for  $M < M_{thresh}$  and that the real part of one eigenvalue became positive for  $M > M_{thresh}$ , indicating that the MOE becomes unstable for larger morphine concentrations. This is consistent with the viral species switch presented in Section 3.2, in which the larger values of M allow the wild-type virus to dominate.

#### 3.3.4. Coexistence equilibrium

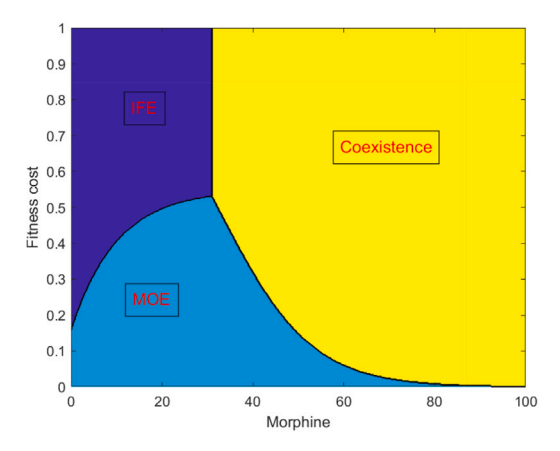
Due to the model's non-linear nature, we could not obtain an analytical expression for the coexistence equilibrium. However, by examining eigenvalues numerically, we determined that the coexistence equilibrium is locally asymptotically stable when  $M > M_{thresh}$ . A high morphine concentration (larger than  $M_{thresh}$ ) allows the wild-type virus to dominate, in which case a small amount of mutant persists due to mutation, resulting in a coexistence equilibrium.

# 3.3.5. Parameter space and stability for equilibrium

In this section, we numerically investigate the effects of F (mutant fitness cost) and B (immune escape rate) on the stability of the model equilibria by examining  $R_0^w$  and  $R_0^m$  under the conditioning of various morphine (M) levels. The stability regions in the M-F and M-B planes are presented in Fig. 5. Depending on the combination of M, F, and B, the model evolves to one of the three biologically relevant equilibria based on local stability analysis: (a) If  $R_0^w < 1$  and  $R_0^m < 1$ , the model converges to the IFE; (b) If  $R_0^w < 1$  and  $R_0^m > 1$ , the model converges to the MOE; and (c) If  $R_0^w < 1$  and  $R_0^w > R_0^m$ , the model converges to the coexistence equilibrium (CE).

In Fig. 5(left) we present the region in the M-F plane, at which each equilibrium is stable. It is interesting to note that the IFE-MOE and MOE-CE boundaries are quite nonlinear. We observe that a lower fitness cost and lower morphine concentration can cause the MOE to be stable. Similarly, a higher fitness cost and lower morphine concentration result in the stability of infection-free equilibrium. For a substantially higher morphine concentration, the coexistence equilibrium becomes stable regardless of fitness cost, promoting both virus species to survive in the system.

In Fig. 5(right), we present the region in the M-B plane for the stability of each equilibrium. In this case, the boundary between the IFE-MOE and MOE-CE is nonlinear, and there is no boundary separating the IFE and CE. As predicted by our model, a smaller B and a lower morphine concentration allow the IFE to become stable. However, a higher B causes the MOE to be stable at a lower level of morphine concentration. Regardless of the escape ratio B, sufficiently high morphine concentration implies the stability of coexistence equilibrium, and both viruses survive in the system.



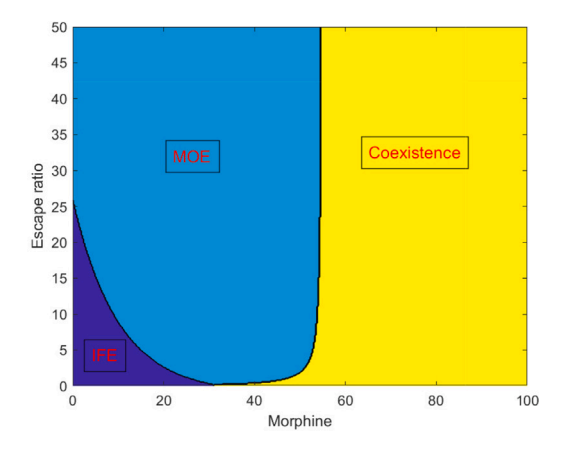


Fig. 5. Model predicted stability regions for Infection-Free Equilibrium (dark-blue), Mutant-Only Equilibrium (light-blue) and Coexistence Equilibrium (yellow) in M - F space (left, with B = 30) and M - B space (right, with F = 0.1).

In summary, a high morphine concentration favors the wild-type virus regardless of other parameter values. Since some mutant virus is always produced from the wild-type, this makes CE the stable equilibrium. The MOE is stabilized by low morphine, a low fitness cost, and high chance of immune escape. At a sufficiently lower morphine concentration, high fitness cost and low escape ratio result in a stable IFE, thereby controlling the infection.

#### 3.4. Effects of morphine on virus-cell dynamics: Model simulations

We now present the model simulations to observe the effects of morphine on the virus-cell dynamics. Since  $R_0 > 1$  for our base parameter values, we expect that the infection is established for any concentrations of morphine, as revealed in the simulations (Fig. 6a). We found  $\sim 1.5 \log_{10}$  increase in set-point viral load (Fig. 6a) and  $\sim 300$  count decrease in CD4 (Fig. 6b) for the morphine conditioning of M = 200 compared to the absence of morphine (M = 0), consistent with the experimental results (Kumar et al., 2004).

We also present the dynamics of wild-type and mutant virus in the absence (M=0, Fig. 6c) and presence (M=200, Fig. 6d) of morphine. For M=0, the mutant virus quickly outcompetes the wild-type, and in the long run, the viral load consists entirely of the mutant population, with the wild-type population going extinct (Fig. 6c). If excessive morphine is in the system, i.e., M=200, both virus species co-exist, with the wild-type population dominating the mutant population (Fig. 6d).

To investigate the altered viral dynamics due to the presence of morphine on the effectiveness of antiretroviral therapy (ART), we introduced ART via reverse transcriptase and protease inhibition (Vaidya and Rong, 2017). These drugs can be introduced into our model by performing the following transformations:  $\beta_i \rightarrow (1 - \Phi)\beta_i, i = l, h$ (reverse transcriptase inhibitors), and  $p \rightarrow (1-\Psi)p$  (protease inhibitors), where  $\Phi$  and  $\Psi$  are efficacy of corresponding ARTs. In Fig. 7, we present simulations of a course of ARTs with 90% efficacy initiated at the steady state. In Fig. 7 (left), we present the viral dynamics in the absence and presence of morphine both before and after ART treatment. We observed that the combined morphine effects in our model caused 7 days longer for the viral load to reach the detection limit (50 viral RNA copies per ml) (Fig. 7 left). In Fig. 7 (right), we first simulate the viral dynamics until a steady state with M = 200 (presence of morphine). Once a steady state is reached, we began ART under two conditions: one without morphine (M=0) and another with M = 200. These two conditions represent the first patient who stops taking drugs of abuse once ART begins and the second patient who continues taking drugs of abuse even after ART. This result (Fig. 7 (right)) further confirms that the viral load falls below the detection limit faster when morphine is not present.

# 3.5. Sensitivity of viral load and CD4 + count

Here we investigate the sensitivity of set-point viral load and CD4+ count to parameter changes under various morphine concentrations. For each parameter  $\rho$ , 10,000 values were sampled via LHS from an interval  $[\rho_{min}, \rho_{max}]$  with lower- and upper-bounds chosen to give a wide range of biologically-relevant values (Table 1). After sampling, the PRCCs of rank-transformed data were computed as the Pearson correlation coefficient between the vectors of residuals from the two regression models (the regression between the model output and the remaining parameters and the regression between the selected parameter and the remaining parameters) (Marino et al., 2008).

Fig. 8(a) and (b) show the PRCCs between the parameters and setpoint viral loads for M=0 and M=200, respectively. Similarly, Fig. 8(c) and (d) show the PRCCs between parameters and CD4+ counts for M=0 and M=200, respectively. Total viral load and CD4+ are both positively associated with target cell recruitment  $\lambda$ . Viral load is positively associated with virus production p and negatively associated with the death parameters  $\delta_T$  and  $\delta_V$ . CD4+ counts are most negatively associated with the transition rate r and positively associated with viral clearance  $\delta_V$ .

In the absence of morphine (Fig. 8a), the total viral load is more sensitive to the fitness cost F because the mutant virus is dominant, and a higher fitness cost corresponds to a weaker virus. When morphine is in use (Fig. 8b), the infected cell death rate  $\delta_I$  had a higher global sensitivity as well. Similarly, in the absence of morphine (Fig. 8c), CD4+ counts were more sensitive to F as well as to CTL-related parameters b,  $\omega$ , and  $\delta_C$  compared to the high morphine case (Fig. 8d). This is expected since the lower morphine case has a stronger response by CTLs and those parameters have a larger effect.

# 4. Conclusion

HIV is an ongoing public health problem worldwide, and the recreational use of injection drugs is one of the main risk factors for contracting it (Alcabes and Friedland, 1995). In addition to increasing the risk of contracting HIV, injection drug use has been shown to have several adverse effects, such as a faster progression to AIDS, a higher chance of HIV-related neurological complications, increased set-point viral load, and decreased immune response (Kumar et al., 2004; Hauser et al., 2009). In this study, we developed a mathematical model of HIV dynamics to investigate the effect of drugs of abuse (morphine) on viral load, immune responses, and viral mutation. This model expands on previous models of HIV wild-type-mutant dynamics with the inclusion of morphine-affected mechanisms (Fryer et al., 2010; Konrad et al., 2011; Althaus and DeBoer, 2008; Asquith et al., 2006; Fernandez et al., 2005; Schwartz et al., 2013; Kwon, 2007). We analyzed our model to

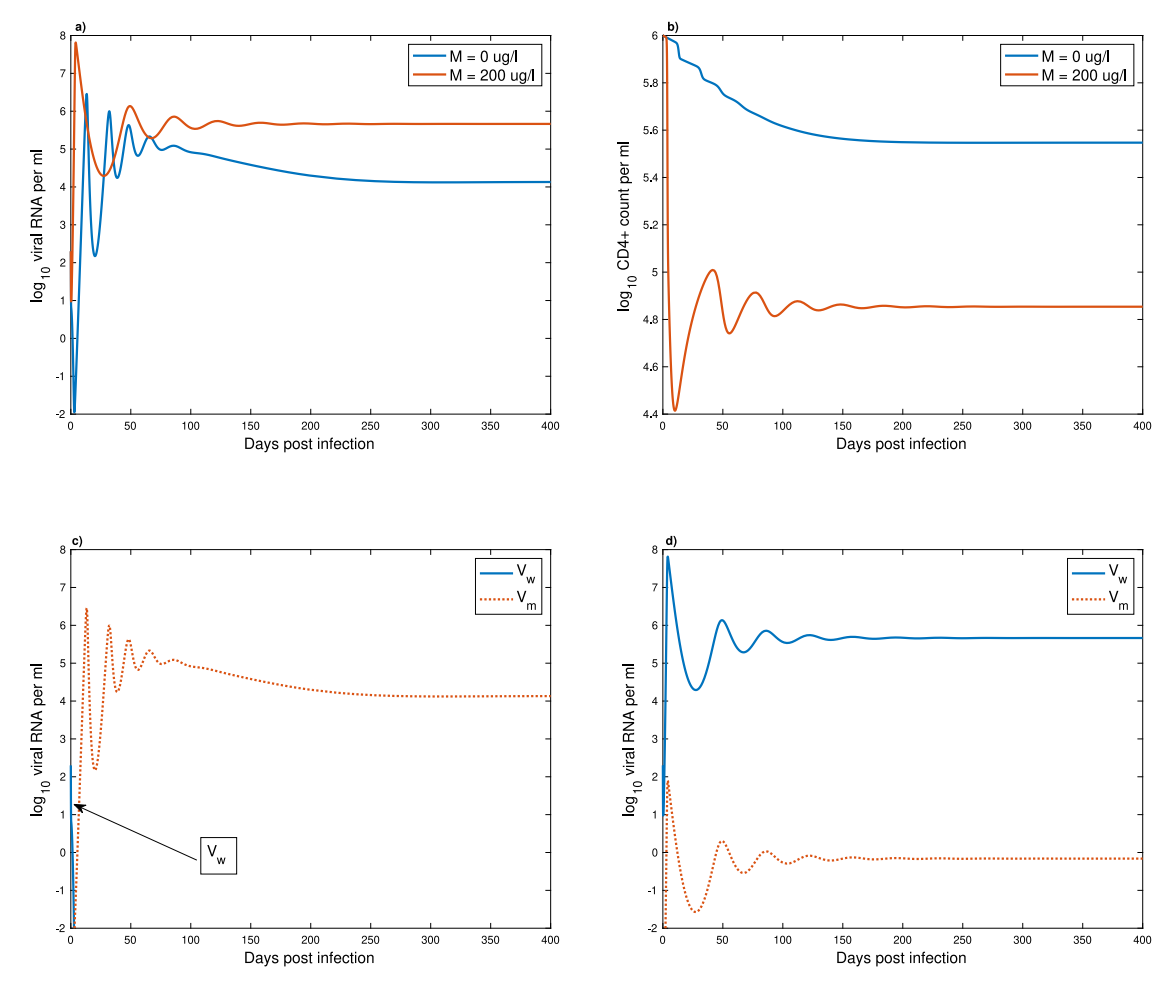


Fig. 6. (a) Model predicted viral load and (b) CD4 + count for 400 days post-infection for absence (M = 0) and presence (M = 200) of morphine. Dynamics of the wild-type and mutant virus populations in (c) the absence (M = 0) and (d) the presence (M = 200) of morphine.

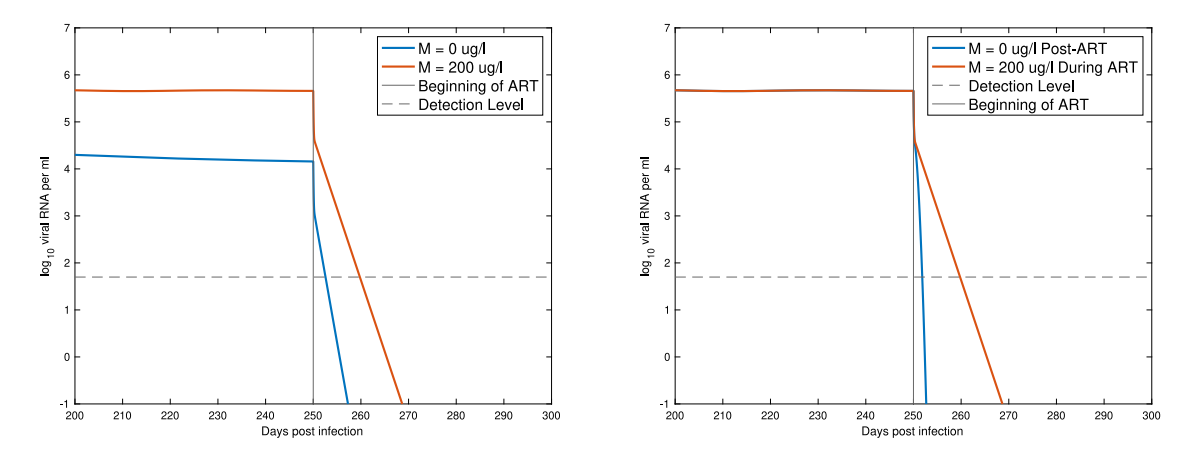


Fig. 7. Model simulation of a course of antiretroviral therapy. (Left) ART was started after the model was allowed to come to steady state. When morphine is not being used (blue), the model predicts a 2 day lag for the virus to become undetectable versus 9 days when morphine is being used (red). (Right) After reaching the steady state under morphine conditioning, ART was initiated with two conditions: one in the absence of post-ART morphine (blue) and another in the presence of post-ART morphine (red).

determine the short- and long-term outcome of an HIV infection in the presence of drugs of abuse.

We identified three biologically-relevant equilibria of our model and characterized their stability in terms of the morphine level present in the system, the fitness cost of mutation of the virus, and the viral escape ratio. Using numerical techniques, we were able to identify the threshold morphine concentration that determines whether the wild-type or mutant virus dominates,  $M_{thresh}$ . We also found  $\sim 1.5 \, \log_{10}$ 

increase in set-point viral load and  $\sim\!300$  count decrease in CD4 when morphine was present in the body of an infected host.

Since morphine inhibits CTL responses, our model predicted a higher set-point viral load in the presence of morphine. Notably, our model showed that wild-type virus dominates in morphine conditioning due to a diminished viral mutation caused by morphine. We also found that a low fitness cost and high escape ratio lead to a state where the wild-type virus goes extinct as the mutant virus out-competes, and

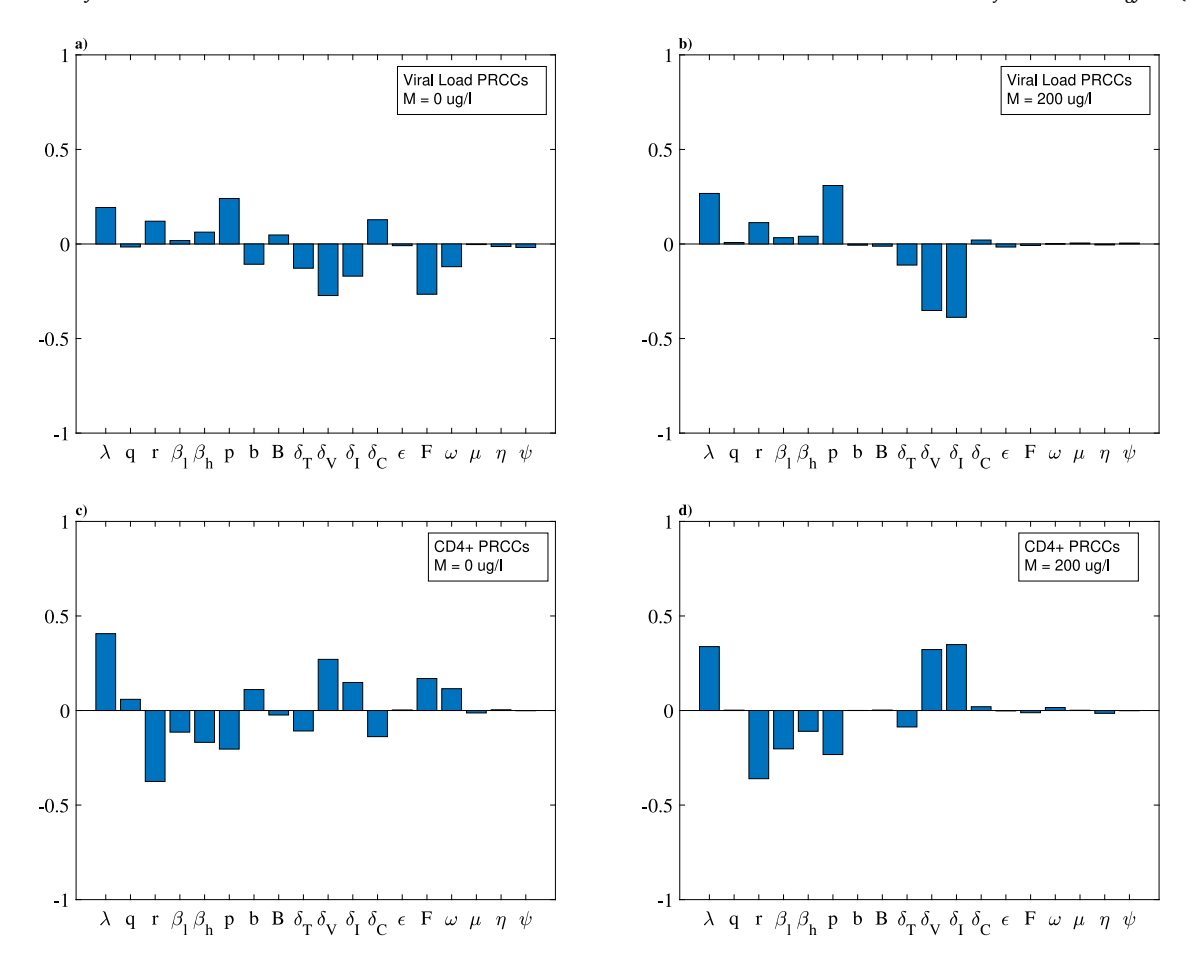


Fig. 8. The partial rank correlation coefficients obtained from Latin hypercube sampling method for set-point viral load (a,b) and CD4 + count (c,d) in the absence (M = 0) and in the presence (M = 200) of morphine.

the virus population is entirely mutant (the mutant-only equilibrium). On the other hand, high morphine gives an advantage to the wild-type virus, increasing the total viral load with the wild-type virus dominating.

Several clinically relevant insights can be gleaned from our model. Our model prediction related to competition dynamics of two viral species influenced by drug use has not been studied experimentally; the results in this paper may motivate such clinical work. A longer time for viral suppression due to ART treatment for morphine conditioning provides important implications for designing treatment protocols for drug-addicted individuals. Other modeling studies with wild-type and mutant viruses have investigated treatment strategies when the mutant is resistant to ART (Kwon, 2007). One of the bases of our model presented here is the decrease in viral mutation due to morphine (Noel et al., 2006; Noel and Kumar, 2007). Our modeling results can also be relevant to the potential reduction of the emergence of ART resistance in the drug-addicted group, thereby providing useful information for successful treatment strategies for drug abusers.

Our model has several limitations. The body metabolizes morphine, and its concentration decreases over time (Olkkola et al., 1988). We assumed a constant morphine concentration, M, and used this value in the analysis of the model. Future work should include time-dependent concentrations using the pharmacokinetics of morphine. Additionally, long-term infection dynamics may be impacted by antibody responses and the presence of latently infected cells (Conway and Perelson, 2015; Mutua et al., 2019). Including these factors in the model may improve our understanding of viral dynamics and mutation under morphine

conditioning. Based on previous studies on HIV, we only considered the fitness cost of mutation. If there is a chance that mutation can result in a more fit mutant with an additional advantage over the wild-type, future investigations may need to consider viral mutation with virus species of various fitnesses. Our model assumed the increased viral load under morphine conditioning is only related to morphine use, as adopted in the experiments. However, we acknowledge that more severe disease could also be due to other factors related to drug use, such as poor diet or lifestyle. Also, further experimental data with frequent measurement of viral loads, virus species populations, and CTLs may help strengthen those effects of morphine introduced into the model.

To summarize, we developed a novel model to investigate the effects of morphine on within-host dynamics of wild-type and mutant HIV species. Our model predicts that the role of morphine in increased susceptibility of the target cells, decreased CTL responses, and decreased mutation eventually results in an increase in set-point viral load and a decrease in CD4 count. We identified three biologically relevant steady states of our model and characterized them based on morphine concentration, the fitness cost of mutation, and viral escape. Our results may help design proper control measures for HIV infection within drug abusers.

# CRediT authorship contribution statement

**Peter M. Uhl:** Modeling, Analysis, Computation, Writing. **Naveen K. Vaidya:** Conceptualization and design, Modeling, Analysis, Supervision, Writing.

#### Declaration of competing interest

The authors declare that they have no known competing financial interests or personal relationships that could have appeared to influence the work reported in this paper.

#### Acknowledgments

This work was funded by NSF, United States grants DMS-1951793, DMS-1836647, and DMS-1616299 from National Science Foundation, the United States, and the UGP award and the start-up fund (NKV) from San Diego State University, United States. The funders had no role in study design, data collection, analysis, decision to publish, or manuscript preparation.

#### References

- Adams, B.M., Banks, H.T., Davidian, M., Kwon, H.-D., Tran, H.T., Wynne, S.N., Rosenberg, E.S., 2005. Hiv dynamics: modeling, data analysis, and optimal treatment protocols. J. Comput. Appl. Math. 184 (1), 10–49.
- Alcabes, P., Friedland, G., 1995. Injection drug use and human immunodeficiency virus infection. Clin. Infect. Dis. 20, 1467–1479.
- Althaus, C.L., DeBoer, R.J., 2008. Dynamics of immune escape during HIV/SV infection. PLoS Comput. Biol. 4 (7), e1000103.
- Asquith, B., Edwards, C.T., Lipsitch, M., McLean, A.R., 2006. Inefficient cytotoxic T lymphocyte-mediated killing of HIV-1-infected cells in vivo. PLoS Biol. 4 (4), e90.
- Barouch, D.H., Kunstman, J., Glowczwskie, J., Kunstman, K.J., Egan, M.A., Peyerl, F.W., Santra, S., Kuroda, M.J., Schmitz, J.E., Beaudry, K., Krivulka, G.R., Lifton, M.A., Gorgon, D.A., Wolinsky, S.M., Letvin, N.L., 2003. Viral escape from dominant simian immunodeficiency virus epitope-specific cytotoxic T lymphocytes in DNA-caccinated rhesus monkeys. J. Virol. 77, 7367–7375.
- Boutwell, C.L., Rolland, M.M., Herbeck, J.T., Mullins, J.I., Allen, T.M., 2010. Viral evolutions and escape during acute HIV-1 infection. J. Infect. Dis. 202, S309–S314.
- Castillo-Chavez, C., Feng, Z., Huang, W., 2002. Mathematical Approaches for Emerging and Reemerging Infections Diseases: An Introduction, first ed. Springer-Verlag, New York, pp. 229–250.
- Chan, D.C., Kim, P.S., 1998. HIV entry and its inhibition. Cell 93, 681-684.
- Chubb, M.C., Jacobsen, K.H., 2010. Mathematical modeling and the epidemiological research process. Eur. J. Epidemiol. 25, 13–19.
- Conway, J.M., Perelson, A.S., 2015. Post-treatment control of HIV infection. Proc. Natl. Acad. Sci. USA 112, 5467–5472.
- DeBoer, R.J., Perelson, A.S., 1998. Target cell limited and immune control models of HIV infection: A comparison. J. Theoret. Biol. 190, 201–214.
- Deng, L., Pertea, M., Rongvauz, A., Want, L., Durand, C.M., Ghiaur, G., Lai, J., McHugh, H.L., Hao, H., Margolick, J.B., Gurer, C., Murphy, A.J., Valenzuela, D.M., Yancopoulus, G.D., Deeks, S.G., Stowig, T., Kumar, P., Siliciano, J.D., Salzberg, S.L., Flavell, R.A., Shan, L., Siliciano, R.F., 2015. Broad CTL response is required to clear latent HIV-1 due to dominance of escape mutations. Nature 381–385.
- Diekmann, O., Heesterbeek, J.A.P., Roberts, M.G., 2009. The construction of next-generation matrices for compartmental epidemic models. J. R. Soc. Interface 7, 873–875
- Fauci, A.S., 2007. Pathogensis of HIV disease: Opportunities for new prevention interventions. Clin. Infect. Dis. 45, \$206–\$212.
- Fernandez, C.S., Stratov, I., De Rose, R., Walsh, K., Dale, C.J., Smith, M.Z., Agy, M.B., Hu, S.L., Krebs, K., Watkins, D.I., O'Connor, D.H., Davenport, M.P., Kent, S.J., 2005. Rapid viral escape at an immunodominant simian-human immunodeficiency virus cytotoxic T-lymphocyte epitope exacts a dramatic fitness cost. J. Virol. 79 (9), 5721–5731.
- Fryer, H.R., Frater, J., Duda, A., Roberts, M.G., 2010. SPARTAC trial inverstigators; phillips, r. e.; mclean, a. r. Modelling the evolution and spread of HIV immune escape mutants. PloS Pathog. 6.
- Fuggetta, M.P., Di Francesco, P., Falchetti, R., Cottarelli, A., Rossi, L., Tricarico, M., Lanzilli, G., 2005. Effect of morphine on cell-mediated immune responses of human lymphocytes against allogeneic malignant cells. J. Exp. Clin. Cancer Res. 24 (2), 255–263.
- Ganusov, V.V., DeBoer, R.J., 2006. Estimating costs and benefits of CTL escape mutations in SIV/HIV infection. PloS Comput. Biol. 3, e24.
- Ganusov, V.V., Goonetilleke, N., Liu, M.K.P., Ferrari, G., Shaw, G.M., McMichael, A.J., Borrow, P., Korber, B.T., Perelson, A.S., 2011. Fitness costs and diversity of the cytotoxic t lymphocyte (CTL) response determine the rate of CTL escape during acute and chronic phases of HIV infection. J. Virol. 85, 10518–10528.
- Ganusov, V.V., Neher, R.A., Perelson, A.S., 2013. Mathematical modeling of escape of HIV from cytotoxic T lymphocyte responses. J. Stat. Mech. 2013, P01010.
- Greenough, T.C., Brettler, D.B., Somasundaran, M., Panicali, D.L., Sullivan, J.L., 1997. Human immunodeficiency virus type 1- specific cytotoxic T lymphocytes (CTL), virus load, and CD4 T cell loss: evidence supporting a protective role for CTL in vivo. J. Infect. Dis. 176, 118–125.

- Hauser, K.F., Hahn, Y.K., Adjan, V.V., Zou, S., Buch, S.K., Nath, A., Bruce-Kelle, A.J., Knapp, P.E., 2009. HIV-1 tat and morphine have interactive effects on oligodendrocyte survival and morphology. Glia 57, 194–206.
- Jordan, D.W., Smith, P., 1999. Nonlinear Ordinary Differential Equations: An Introduction to Dynamical Systems, third ed. Oxford University Press, New York.
- Kileen, N., Davis, C.B., Chu, K., Crooks, M.E.C., Sawada, S., Scarborough, J.D., Boyd, K.A., Stuart, S.G., Xu, H., Littman, D.R., 1993. CD4 function in thymocyte differentiation and T cell activation. Philos. Trans. R. Soc. Lond. B Biol. Sci. 342, 25–34.
- Kitchen, S.G., Whitmire, J.K., Jones, N.R., Galic, Z., Kitchen, C.M.R., Ahmed, R., Zack, J.A., Chisari, F.V., 2005. The CD4 molecule on CD8+ T lymphocytes directly enhances the immune response to viral and cellular anitgens. Proc. Natl. Acad. Sci. USA 102, 3794–3799.
- Klein, M.R., van der Burg, S.H., Pontesilli, O., Miedema, F., 1998. Cytotoxic T lymphocytes in HIV-1 infection: a killing paradox? Immun. Today 19, 317–324.
- Kohli, R., Lo, Y., Howard, A.A., Buono, D., Floris-Moore, M., Klein, R.S., Schoenbaum, E.E., 2005. Mortality in an urban cohort of HIV-infected and at-risk drug users in the era of highly active antiretroviral therapy. Clin. Infect. Dis. 41, 864–872.
- Konrad, B.P., Vaiyda, N.K., Smith?, R.J., 2011. Modeling mutation to a cytotoxic T-lymphocyte HIV vaccine. Math. Popul. Stud. 18, 122–149.
- Kumar, R., Torres, C., Yamamura, Y., Rodriguez, I., Martinez, M., Staprans, S., Donahoe, R.M., Kraiselburd, E., Stephens, E.B., Kumar, A., 2004. Modulation by morphine of viral set point in rhesus macaques infected with simian immunodeficiency virus and simian-human immunodeficiency virus. J. Virol. 78, 11425–11428.
- Kwon, H.-D., 2007. Optimal treatment strategies derived from a HIV model with drug-resistant mutants. Appl. Math. Comput. 188 (2), 1193–1204.
- Li, Y., Wang, X., Tian, S., Guo, C., Douglas, S.D., Ho, W., 2002. Methadone enhances human immunodeficiency virus infection of human immune cells. J. Infect. Dis. 185, 118–122.
- Mansky, L.M., Temin, H.M., 1995. Lower in vivo mutation rate of human immunodeficiency virus type 1 than that predicted from the fidelity of purified reverse transcriptase. J. Virol. 69, 5087–5094.
- Marino, S., Hogue, I.B., Ray, C.J., Kirschner, D.E., 2008. A methodology for performing global uncertainty and sensitivity analysis in systems biology. J. Theoret. Biol. 254, 178–196.
- McMichael, A.J., Rowland-Jones, S.L., 2001. Cellular immune responses to HIV. Nature 410. 980–987.
- Miyagi, T., Chuang, L.F., Doi, R.H., Carlos, M.P., Torres, J.V., Chuang, R.Y., 2010. Morphine induces gene expression of antiviral CCR5 in human CEMx174 lymphocytes. J. Biol. Chem. 275, 31305–31310.
- Mutua, J.M., Perelson, A.S., Kumar, A., Vaidya, N.K., 2019. Modeling the effects of morphine altered virus specific antibody responses on HIV/SIV dynamics. Sci. Rep. 0, 5422
- Noel, R., Kumar, A., 2007. SIV vpr evolution is inversely related to disease progression in a morphine-dependent rhesus macaque model of AIDS. Virology 359, 397–404.
- Noel, R., Marrero-Otero, Z., Kumar, R., Chompre-Gonzalez, G.S., Verma, A.S., Kumar, A., 2006. Correlation between SIV tat evolution and AIDS progression in cerebrospinal fluid of morphine-dependent and control macaques infected with SIV and SHIV. Virology 349, 440–452.
- Olkkola, K.T., Maunuksela, E., Korpela, R., Rosenberg, P.H., 1988. Kinetics and dynamics of postoperative intravenous morphine in children. Clin. Pharmacol. Ther. 44, 128–136.
- Perelson, A.S., Ribeiro, R.M., 2013. Modeling the within-host dynamics of HIV infection. BMC Biol. 11.
- Perera, S.D., Perera, S.S.N., Jayasinghe, S., 2006. Modeling and sensitivity of dengue viral dynamics. Int. J. Curr. Res. 8, 34899–34906.
- Perko, L., 1991. Differential Equations and Dynamical Systems, second ed. Springer-Verlag, New York.
- Ramratnam, B., Bonhoeffer, S., Binley, J., Hurley, A., Zhang, L., Mittler, J.E., Markowitz, M., Moore, J.P., Perelson, A.S., Ho, D.D., 1999. Rapid production and clearance of HIV-1 and hepatitis c virus assessed by large volume plasma apheresis. Lancet 354, 1782.
- Ribeiro, R.M., Chavez, L.L., Li, D., Self, S.G., Perelson, A.S., 2010. Estimation of the initial viral growth rate and basic reproductive number during acute HIV-1 infection. J. Virol. 84, 6096–6102.
- Rivera-Amill, V., Silverstein, P.S., Noel, R., Kumar, S., Kumar, A., 2014. Morphine and rapid disease progression in nonhuman primate model of AIDS: Inverse correlation between disease progression and virus evolution. J. Neuroimmune Pharm. 5, 122–132.
- Rodrigues, H.S., Monteiro, M.T.T., Torres, D.F.M., 2013. Sensitivity analysis in a dengue epidemiological model. Conf. Pap. Math. 2013, 721406.
- Schwartz, E.S., Biggs, K.R.H., Bailes, C., Ferolito, K.A., Vaidya, N.K., 2016. HIV dynamics with immune responses: Perspectives from mathematical modeling. Curr. Clin. Microbiol. Rep. 3, 216–224.
- Schwartz, E.J., Yang, O.O., Cumberland, W.G., de Pillis, L.G., 2013. Computational model of HIV-1 escape from the cytotoxic T lymphocyte response. Can. Appl. Math. Q. 21 (2), 261–279.

- Stafford, M.A., Corey, L., Cao, Y., Daar, E.S., Ho, D.D., Perelson, A.S., 2000. Modeling plasma virus concentration during primary HIV infection. J. Theoret. Biol. 203, 285–301.
- Tarfulea, N.E., 2017. A mathematical model for CTL effect on a latently infected cell inclusive HIV dynamics and treatment. AIP Conf. Proc. 1895 (1), 070005. UNAIDS, 2021. UNAIDS data 2021.
- Vaidya, N.K., Peter, M., 2021. Modeling intracellular delay in within-host HIV dynamics under conditioning of drugs of abuse. Bull. Math. Biol. 83, 81.
- Vaidya, N.K., Ribeiro, R.M., Perelson, A.S., Kumar, A., 2016. Modeling the effects of morphine on simian immunodeficiency virus dynamics. PloS Comput. Biol. 12, e1005127.
- Vaidya, V.K., Rong, L., 2017. Modeling pharmacodynamics on HIV latent infection: Choice of drugs is key to successful cure via early therapy. SIAM J. Appl. Math. 77, 1781–1804.